

Digital Microfabrication of User-Defined 3D Microstructures in Cell-Laden Hydrogels

Pranav Soman,¹ Peter H. Chung,¹ A. Ping Zhang,^{1,2} Shaochen Chen¹

¹Department of NanoEngineering, University of California, San Diego, 9500 Gilman Drive, SME Building, MC-0448, La Jolla, CA, 92093; telephone: 858-822-7856; fax: 858-534-9553; e-mail: chen168@ucsd.edu

²Department of Electrical Engineering, The Hong Kong Polytechnic University, Kowloon, Hong Kong SAR, China

ABSTRACT: Complex 3D interfacial arrangements of cells are found in several *in vivo* biosystems such as blood vasculature, renal glomeruli, and intestinal villi. Current tissue engineering techniques fail to develop suitable 3D microenvironments to evaluate the concurrent effects of complex topography and cell encapsulation. There is a need to develop new fabrication approaches that control cell density and distribution within complex 3D features. In this work, we present a dynamic projection printing process that allows rapid construction of complex 3D structures using custom-defined computer-aided-design (CAD) files. Gelatin-methacrylate (GelMA) constructs featuring user-defined spiral, pyramid, flower, and dome micro-geometries were fabricated with and without encapsulated cells. Encapsulated cells demonstrate good cell viability across all geometries both on the scaffold surface and internal to the structures. Cells respond to geometric cues individually as well as collectively throughout the larger-scale patterns. Time-lapse observations also reveal the dynamic nature of mechanical interactions between cells and micro-geometry. When compared to conventional cell-seeding, cell encapsulation within complex 3D patterned scaffolds provides long-term control over proliferation, cell morphology, and geometric guidance. Overall, this biofabrication technique offers a flexible platform to evaluate cell interactions with complex 3D micro-features, with the ability to scale-up towards high-throughput screening platforms.

Biotechnol. Bioeng. 2013;110: 3038–3049.

© 2013 Wiley Periodicals, Inc.

KEYWORDS: cell encapsulation; 3D micro-architecture; digital microfabrication; gelatin-based hydrogel

Introduction

For tissue engineering to become a viable approach for regenerative medicine and eventual organ replacement, cells and their supporting medium must be orchestrated to replicate the inherent structure and activity fundamental to their *in vivo* function (Kirkpatrick et al., 2011). To this end, methods for incorporating cells within biomaterial constructs have evolved to allow for greater precision and flexibility in arranging cells within their scaffold environment (Chan et al., 2010; Du et al., 2008; Kaji et al., 2011; Miller et al., 2012). Two-dimensional patterning of substrates has been employed extensively to direct cell arrangement and proliferation, and numerous methods have been developed to create complex surface geometries and multicellular configurations. Initial approaches towards cell patterning were partially motivated by the shortcomings of earlier co-culture systems. These multicellular models were typically developed via deposition (i.e., “seeding”) of two or more cells types (Bhatia et al., 1999; Kane et al., 1999). However, the random distributions resulting from cell-seeding prevented precise control over the degree and nature of cell–cell contact. To address this limitation, photolithographic methods have been used to pattern adhesive regions on a substrate to localize multiple cell types and enable mechanistic studies related to either homotypic or heterotypic cell interactions (Bhatia et al., 1999). Due to its reliance on specific cell–adhesive protein interactions, this approach requires the careful selection of cell type, adhesive protein, and optimal substrate. Soft lithography and associated micro-contact printing techniques have been extensively used to attain precise control over the deposition of adhesive proteins and, as an extension, cellular patterning (Chen et al., 1997; Kane et al., 1999). Microfluidic strategies have also been employed, usually in combination with micro-contact printing, to

Pranav Soman and Peter H. Chung are contributed equally to this work.

Correspondence to: S. Chen

Contract grant sponsor: National Institute of Biomedical Imaging and Bioengineering

Contract grant number: R01EB012597

Contract grant sponsor: National Science Foundation (NSF)

Grant numbers: CMMI-1120795; CMMI-1130894

Contract grant sponsor: NSF Graduate Research Fellowship

Contract grant number: DGE-1144086

Contract grant sponsor: UCSD Neuroscience Microscopy Shared Facility

Contract grant number: P30 NS047101

Received 5 February 2013; Revision received 15 April 2013; Accepted 29 April 2013

Accepted manuscript online 18 May 2013;

Article first published online 3 June 2013 in Wiley Online Library

(<http://onlinelibrary.wiley.com/doi/10.1002/bit.24957/abstract>).

DOI 10.1002/bit.24957

pattern heterogeneous cell populations (Torisawa et al., 2009). Other innovative techniques have used light (Kikuchi et al., 2009), electrical stimuli (Fan et al., 2008), and heat (Elloumi Hannachi et al., 2009) as triggers to control cell–substrate interaction in real time. Interlocking silicon substrates have also been microfabricated to dynamically modulate cell–cell contact in investigations of paracrine and juxtacrine cell-signaling (Hui and Bhatia, 2007).

Most of these aforementioned approaches focus mainly on patterning adhesive proteins, and cells are typically introduced via traditional cell-seeding techniques after scaffold fabrication. In comparison, newer strategies of three-dimensional cell patterning aim to arrange cells in sophisticated 3D geometries by incorporating cells *within* a scaffold during fabrication. Co-culture models have been generated by directing cell-laden microengineered hydrogels to assemble in a controlled fashion (Du et al., 2008). Direct-writing techniques, often referred to as free-form fabrication or rapid prototyping, can be used to print multiple cell types in 3D (Boland et al., 2006; Malone and Lipson, 2007; Mironov et al., 2007; Ovsianikov et al., 2010). Typically, these computer-assisted manufacturing approaches recreate a 3D scaffold by translating either the computer-controlled stage or the deposition device in the XYZ directions according to a user-defined 3D model. This approach allows incorporation of living cells and other biomolecules within the liquid prepolymer solution. The distinction between 3D patterning of a scaffold substrate versus 3D encapsulation of cells within the scaffold should be noted: patterning of complex surface geometries does not necessarily yield an environment representative of *in vivo* architecture if the cells are only incorporated via seeding. This approach still yields a monolayer culture in a comparatively contrived environment due to the stark boundary formed between the substrate and the surrounding culture media. Cell seeding techniques can also yield inconsistencies in cell distribution throughout the scaffold surface due to cell aggregation. The preferential deposition of cells that results within certain geometric features, such as large wells or valleys, can confound investigations attempting to determine the independent influence of geometric cues on cell behavior. Recent evidence demonstrates that distributing cells three-dimensionally throughout a substrate can yield significant differences in cellular response to exogenous cues (e.g., during high-throughput drug screening) when compared with 2D monolayer culture (Fralely et al., 2010; Wirtz et al., 2011; Zaman et al., 2006). Further differences have been observed in cell morphology, cell–cell communication, and cell–ECM interactions (Cukierman et al., 2002; Loessner et al., 2010). Additionally, as embedding cells within a 3D hydrogel can allow for their immobilization and subsequent controlled release, these novel culture systems may better replicate the spatiotemporal presentation of cells to each other throughout the developmental process (Fischbach et al., 2009; Pampaloni et al., 2007; Tibbitt and Anseth, 2009). Notwithstanding these advantages, 3D encapsulation of living cells within complex user-defined features remains a challenge.

Photolithographic and soft lithographic techniques have become mainstays of traditional hydrogel patterning and are well suited to produce 2D microstructures, in addition to some 3D structures with simple geometries and aspect ratios. Using these approaches, many researchers have demonstrated how various processing methods can be used to mold soft cell-laden hydrogel scaffolds while tailoring their bulk mechanical properties to direct the physiology of encapsulated cells (Nichol et al., 2010; Nicodemus and Bryant, 2008; Soman et al., 2012; Williams et al., 2005; Yeh et al., 2006). Other groups have utilized these techniques in stiffer materials to generate surface topographies that can influence cell growth, activity, and fate (Dalby et al., 2007; Fu et al., 2010; Jeon et al., 2010; Kulangara and Leong, 2009; Yu et al., 2012). However, these topographic effects have only been investigated for seeded cells, as current cell encapsulation techniques are limited to simpler bulk geometries in soft, naturally derived biomaterials. Since an increase in feature complexity generally necessitates an increase in material stiffness, translating sophisticated biomimetic geometries from stiff materials to softer biopolymers remains an important challenge. These limitations are borne out of fundamental material requirements that are often competing: (1) soft biomaterial substrates with high water content are needed to support cell viability, and (2) polymers must be robust enough to faithfully reproduce the specified features while withstanding current fabrication techniques. Thus, most cell-encapsulation approaches cannot incorporate the complex geometries representative of native anatomy, and those that can (e.g., bio-inkjet printing or 3D plotting) are often labor-intensive and time-consuming, thereby limiting their scalability.

To address the limitations of current techniques in encapsulating cells within complex 3D geometries, we present here a novel, rapid microfabrication approach for constructing cell-laden hydrogel scaffolds that (1) provide complex user-defined 3D geometries composed of a naturally derived biomaterial, (2) allow for consistent 3D distribution of cells encapsulated within the hydrogel, (3) support cell viability and proliferation, (4) feature dynamic, large-scale mechanical cell–scaffold interactions, and (5) yield cell behavior and morphology that contrasts with outcomes from traditional cell seeding. Importantly, these constructs enable control and integration of complex 3D geometries while providing internal 3D distribution of encapsulated cells. The ability to better mimic a native tissue environment by controlling the arrangement of cells within a complex patterned 3D hydrogel will yield broad impact in tissue engineering, drug discovery, and fundamental cell biology research (Kaji et al., 2011; Yu et al., 2012).

Materials and Methods

Biofabrication Using Dynamic Projection Stereolithography

An array of micron-scale features was built in various biopolymers using UV photolithography in a layer-by-layer

fashion as described earlier (Zhang et al., 2012). The main components of the fabrication system are a UV light source (EXFO Omnicure S2000, Quebec, QC, Canada), a digital light processing (DLP) chip (Discovery 4000, Texas Instrument, TX), and computer controlled x - y - z stages (Newport 426/433 series). The wavelength used is 365 nm with a source output of 30 W/cm^2 . User-defined computer-aided-design (CAD) files were transferred to the DLP chip to generate a series of virtual masks. DLP chip modulated images were projected onto a photocurable pre-polymer through a UV-grade optical lens (Edmunds Optics, Barrington, NJ). Areas illuminated by UV light crosslinked immediately, while

leaving the dark regions un-crosslinked, forming an image in a specific polymerization plane. This process is dynamically repeated through a series of user-defined digital masks while the stage is translated to construct scaffolds with precise structure and cellular composition (Fig. 1a). These patterns were irradiated for 35 s at a projected UV intensity of 11 mW/cm^2 .

Methacrylation of Glass Coverslips

Round glass coverslips (12 mm diameter, Chemglass Life Sciences, Vineland, NJ) were agitated in Piranha for 5 min,

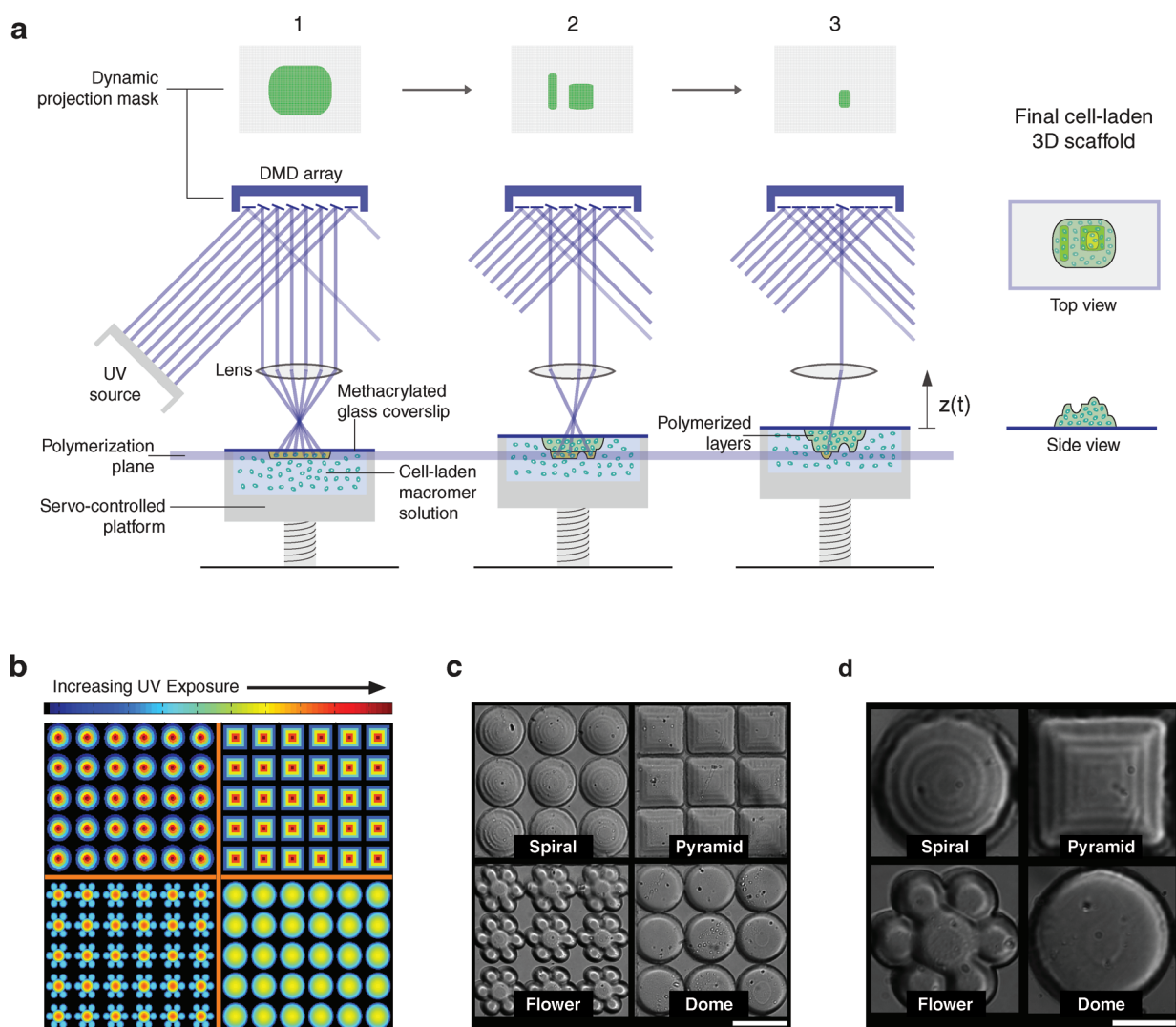


Figure 1. Fabrication method and examples of hydrogels formed via dynamic projection printing. **a:** Cells in a macromer solution are placed in a chamber covered by a methacrylated glass coverslip. Polymerization of the 3D scaffold begins at the coverslip surface, where the reflected UV image from the DMD array is focused [1]. Starting from the bottom portion of the scaffold, which is cross-linked to the coverslip, the complete structure is fabricated in one continuous process. The projection mask on the DMD changes as the servo-controlled platform translates up [2] until the top of the scaffold is reached [3], thereby encapsulating the cells in the user-defined 3D structure. **b:** Heatmap representing the cumulative UV exposure at each part of the pattern. Precise specification of the duration and spatial distribution of UV light allows for the creation of cell-laden structures with complex 3D features at high resolution. **c** and **d:** DIC micrographs of 10% gelatin methacrylate (GelMA) scaffolds fabricated using the dynamic projection printing system. The patterns generated consist of three-dimensional spiral, pyramid, dome, and flower structures [clockwise from top left]. All scale bars are $100 \mu\text{m}$.

washed in DI water three times (5 min each time), and subsequently washed in 100% ethanol (Fisher Scientific, Pittsburgh, PA) and dried with nitrogen. Dried glass coverslips were functionalized in a bath containing 85 mM 3-(Trimethoxysilyl)propyl methacrylate (Fluka, St. Louis, MO) in ethanol with acetic acid (pH 4.5) while rocking overnight at room temperature. The coverslips were washed with ethanol (three times, 5 min each time), dried with nitrogen, and baked for 1 h.

Pre-Polymer Synthesis

Gelatin methacrylate (GelMA) was synthesized as described in previous reports (Gauvin et al., 2012; Nichol et al., 2010). Briefly, porcine skin gelatin (Sigma–Aldrich, St. Louis, MO) was mixed at 10% (w/v) in phosphate buffered saline (PBS; Gibco, Billings, MT) and stirred at 60°C until fully dissolved. Methacrylic anhydride (MA; Sigma) was added to the solution at a rate of 0.5 mL/min until a concentration of 8% (v/v) of MA was obtained in the gelatin solution. The solution was then stirred for 3 h at 60°C. Following a 2X dilution with warm PBS, the solution was dialyzed against distilled water using 12–14 kDa cutoff dialysis tubing (Spectrum Laboratories, Rancho Dominguez, CA) for 1 week at 40°C to remove the unreacted groups from the solution. The dialyzed GelMA solution was sterile filtered (0.2 μm), frozen overnight at –80°C, and lyophilized in a freeze dryer (Labconco, Kansas City, MO) for 1 week. Freeze-dried GelMA foam was stored at –80°C until further usage. A 15% (w/v) GelMA macromer solution was prepared by mixing the freeze-dried GelMA with Dulbecco's Modified Eagle Medium supplemented with 10% bovine calf serum or fetal bovine serum (HyClone, Logan, UT) at 40°C until fully dissolved. Photoinitiator (0.3%, w/v, Irgacure 2959, CIBA Specialty Chemicals, Basel, Switzerland) was added to the solution to allow for photopolymerization with efficient cure depth and optimal pattern resolution. In the final preparation, the 15% GelMA solution was mixed with either a cell suspension (for cell encapsulation) or additional cell-free media (for cell seeding on blank scaffolds) to achieve a final concentration of 10% (w/v) GelMA.

Cell Culture and Immunohistochemical Staining

NIH-3T3 murine embryonic fibroblasts (3T3s) and C3H/10T1/2 murine mesenchymal progenitor cells (10T1/2s) were purchased from ATCC and cultured according to the protocols provided by ATCC. NIH/3T3 cells were cultured in Dulbecco's Modified Eagle Medium (DMEM, Gibco) supplemented with 10% bovine calf serum, heat inactivated (BCS, HyClone), and 1% penicillin–streptomycin. 10T1/2 cells were cultured in DMEM supplemented with 10% fetal calf serum, heat inactivated (FBS, HyClone). Both cell types were maintained in a 37°C incubator with 5% CO₂. Cells were passaged using standard cell culture protocols using 0.25% Trypsin/EDTA and were used within passage number 12. Cells were harvested and counted based on the general protocol and then either encapsulated or seeded onto the

scaffold with their respective growth media. Media were initially changed 1 day after seeding and then refreshed every other day. Cells were fixed at various time points and stained for F-actin (for 3T3s) or α-SM actin (for 10T1/2s) and nuclei. Cell-laden scaffolds were fixed using 4% paraformaldehyde (Electron Microscopy Sciences, Fort Washington, PA) for 15 min at room temperature and permeabilized with 0.1% Triton X-100 (Sigma–Aldrich) in PBS with 2% bovine serum albumin (BSA, HyClone) for 30 min. For F-actin staining, cells were then exposed to 5 units/mL rhodamine phalloidin (Biotium, Hayward, CA) at room temperature for 30 min. For 10T1/2 staining, permeabilized cells were incubated with primary antibodies for α-SM actin at 4°C overnight, followed by incubation with labeling secondary antibodies (Alexa 488 or Alexa 647, Invitrogen, Carlsbad, CA) at room temperature for 1 h. Nuclei were counterstained with Hoechst 33258 DNA dye (Invitrogen). Confocal fluorescence imaging was performed using an Olympus FV1000 confocal microscope, and image analysis was performed using ImageJ.

Results and Discussion

Scaffold Fabrication

Although natural polymers such as protein-based (e.g., fibrin, gelatin) or polysaccharide-based (e.g., hyaluronic acid, alginate) biomaterials exhibit favorable cell–material interactions, they are difficult to pattern with conventional photolithographic techniques, especially when complex 3D geometries are involved. Additionally, the post-processing and curing steps often used to improve mechanical stability in hydrogel scaffolds can be cytotoxic and thereby preclude the simultaneous incorporation of cells during fabrication. We have developed a dynamic projection printing process that allows rapid construction of complex 3D structures while maintaining highly specified features by eliminating the need for a secondary mold to cast the scaffold (Zhang et al., 2012). User-defined computer-aided-design (CAD) files were used to generate a series of virtual masks, which were used to project UV light onto a photocurable gelatin-based prepolymer to construct scaffolds with complex 3D architectures (Fig. 1a and b). Gelatin-methacrylate (GelMA) constructs were initially fabricated without encapsulated cells to provide substrates for characterization and comparative cell seeding experiments. The dynamic stereolithographic method yielded 100–250 μm thick scaffolds with features that corresponded to various geometries as specified in the dynamic photomasks: spiral, pyramid, flower, and dome (Fig. 1c and d). Low and high strain bulk moduli of the 10% GelMA scaffolds were 75 and 580 kPa respectively (Gauvin et al., 2012). While synthetic polymers, such as poly(ethylene) glycol, can offer faithful reproduction of complex features, these materials are often stiffer and require the addition of bioactive molecules, such as RGDS peptide sequences, to support cell growth. In contrast, naturally derived GelMA facilitates cell adhesion and proliferation throughout a softer 3D structure via natively available peptide sequences. NIH-

3T3 murine embryonic fibroblasts (3T3s) and C3H/10T1/2 murine mesenchymal progenitor cells (10T1/2s), both at passage numbers less than 12, were incorporated in the pre-polymer solution to provide structures featuring the specified geometries with cells distributed uniformly throughout. The final density of cell distribution within the scaffold correlated to the concentration of cells present in the pre-polymer solution with a $1\text{--}3 \times 10^6$ cells/mL solution providing a

scaffold with a mean cell distribution of 600–1,800 cells/ mm^3 .

Cell Interaction With Scaffold Geometry

Cells were observed throughout long-term culture to determine the extent to which they respond to and interact with their local geometry. In the cell-laden scaffolds, cells

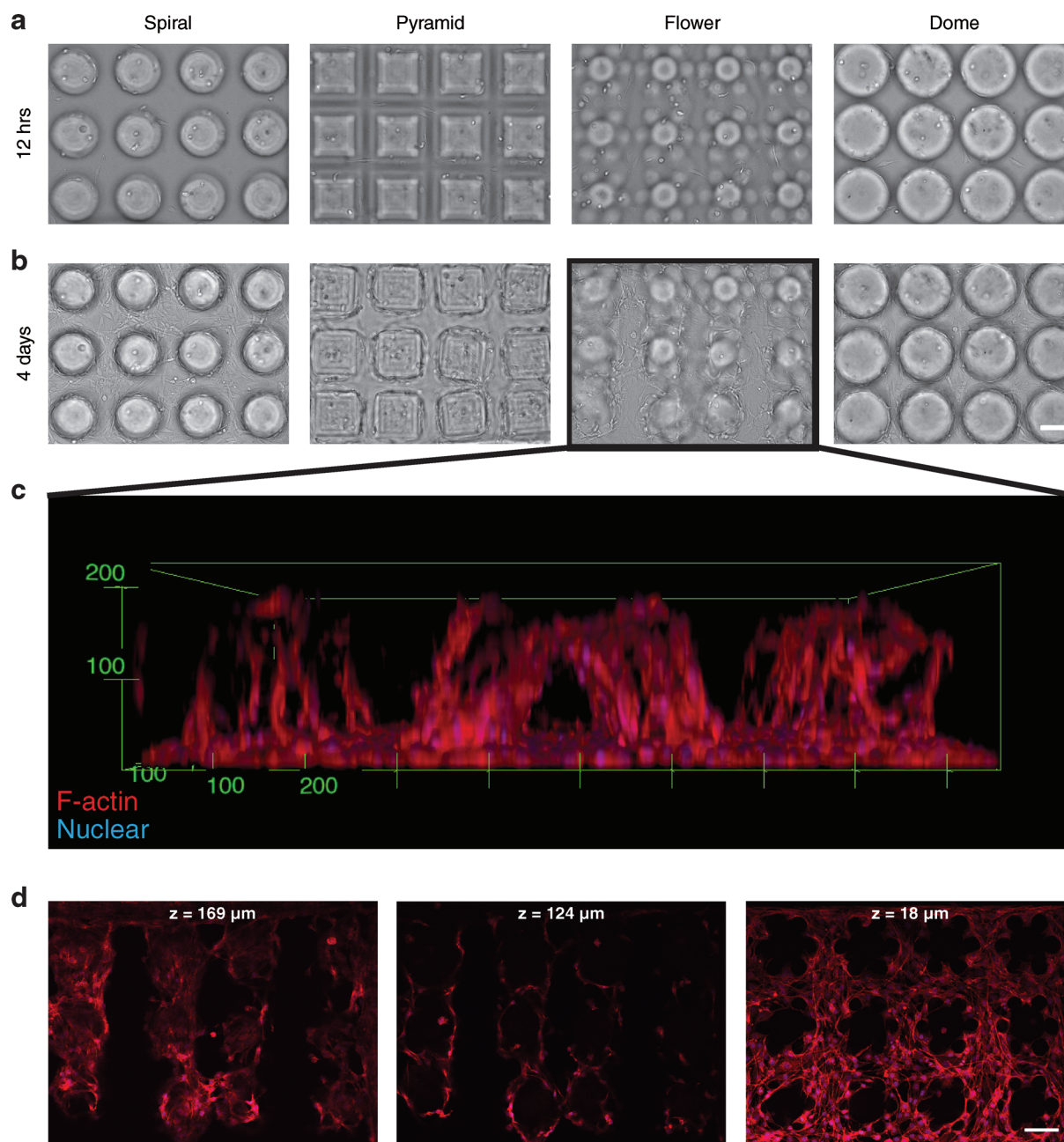


Figure 2. Cells respond to the complex 3D geometric cues and interact dynamically with the GelMA scaffold to remodel the position and shape of the structures. **a:** GelMA scaffolds with encapsulated NIH/3T3 cells at 12 h post-fabrication. **b:** Deformation of the structures as observed 4 days post-encapsulation. **c:** 3D reconstruction of confocal fluorescence micrographs indicates height-dependent deformation of the scaffold as mediated by cell–cell interactions across two flower structures. Cells were stained for F-actin (red) and nuclei (blue). **d:** Individual Z sections of the same flower structures as shown in (c) demonstrate height-dependent deformation when progressing up from the floor to the top of the structures. All scale bars are 100 μm .

respond to complex features and remodel the 3D structure in a dynamic manner (Fig. 2). Multicellular organization of cells was present initially on the perimeter of the structures. Upon continued proliferation, cells covered the entire surface of each structure and branched across structures to create an interconnected network of cells (Supplementary Information Fig. S1). Interestingly, as cells organized between adjacent structures, deformation of the scaffold features was observed, and geometries exhibiting features with smaller radii of curvature (e.g., flower and pyramid) experienced greater deformation of their bulk structures (Fig. 2b). 3D reconstruction of confocal micrographs of the scaffolds after staining for F-actin (red) and nuclei (blue) revealed that deformation of the scaffold features was height-dependent (Fig. 2c). Specifically, cells were able to deform the upper portions of the structures (e.g., features furthest from the

coverslip/base of the scaffold) to a greater extent than the lower portions (Fig. 2d). This selective deformation confirmed that the bulk structure maintained its initial position on the coverslip surface. Though scaffold movement for the spiral and dome structures is not apparent in the still micrographs, time lapse microscopy of these scaffolds at 4 days after fabrication revealed that this dynamic collective mechanical interaction is also present in the spiral structures (Supplementary Information Movie). These results demonstrate the influence that geometry can have on organized multicellular action within a complex 3D scaffold environment.

Encapsulated cells within the GelMA scaffolds exhibited 3D cell spreading at various Z planes throughout the scaffold. The morphology of fully encapsulated 3T3 fibroblasts after long-term culture was observed by staining cells with

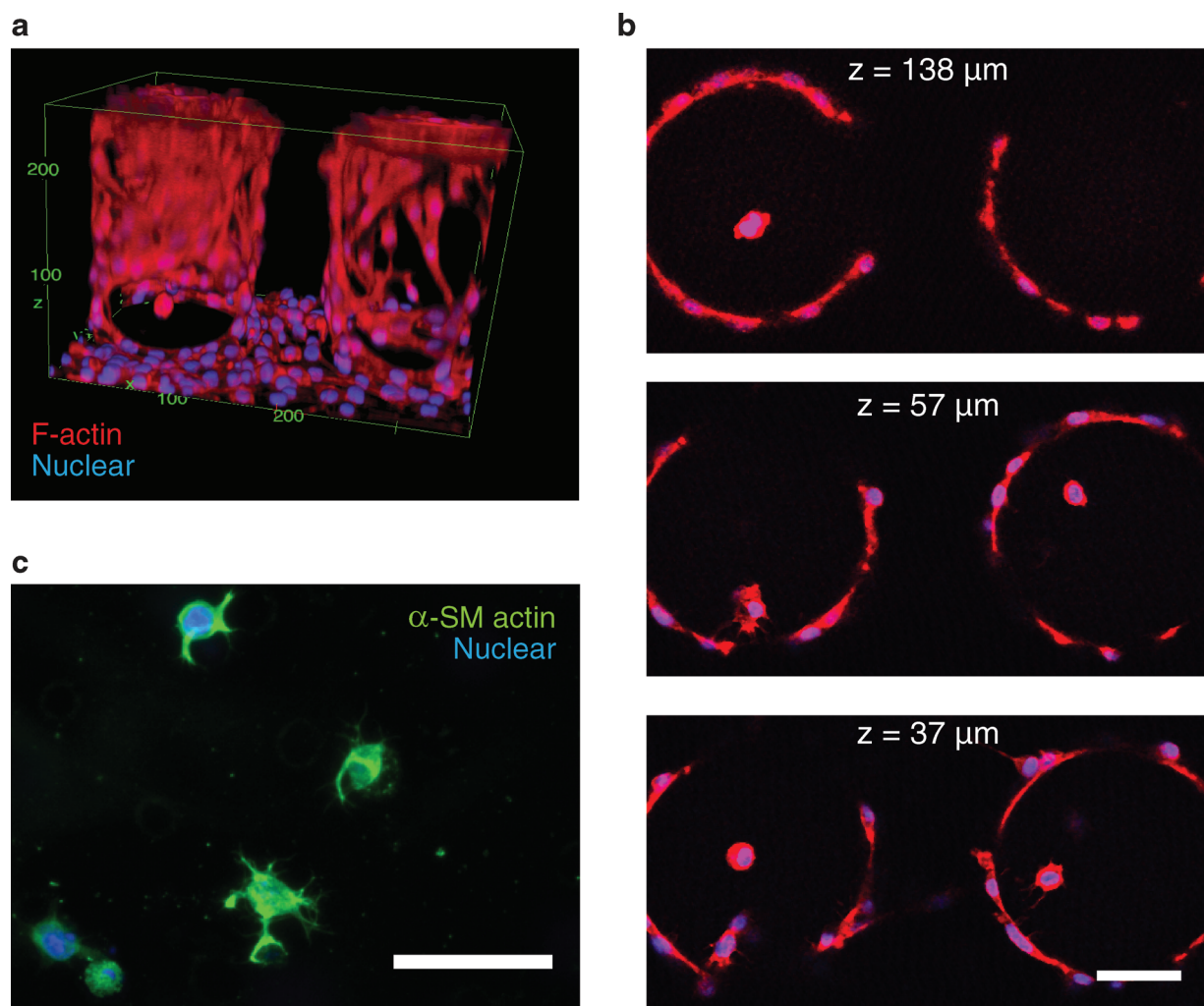


Figure 3. Cells that remain encapsulated within the GelMA scaffolds exhibit 3D cell spreading and maintain active cell-material interactions. Confocal fluorescence micrographs (a) reconstructed in 3D and (b) viewed at various Z planes throughout the scaffold reveal NIH/3T3 fibroblasts on the scaffold surface displaying morphology different from cells internal to the structures. b: Cells that remain embedded within the GelMA scaffold at 4 days post-encapsulation exhibit extension of pseudopodia preferentially towards the surface of the encapsulating structure. Cells were stained for F-actin (red) and nuclei (blue). c: 10T1/2 cells encapsulated within GelMA scaffolds express a smooth muscle cell phenotype, as shown via staining for α -SM actin (green), and maintain cell-material interactions at 8 days post-encapsulation as indicated by 3D projections of pseudopodia. All scale bars are 50 μ m.

rhodamine phalloidin and Hoechst to visualize F-actin and nuclei respectively. 3T3 cells fully embedded within the structures display morphology different from cells external to the structure (i.e., surface cells). Additionally, we observed pseudopod extension in the encapsulated cells as well as in cells on the periphery of the patterned structures. The pseudopodia often crossed the interface between the GelMA structures and the surrounding media, suggesting the continued ability of cells to maintain cell–cell and cell–matrix interactions across this boundary (Fig. 3b). Interestingly, the pseudopodia for encapsulated cells exhibited preferential orientation towards the interface, which may be induced by the presence of a diffusion gradient across the boundary. Encapsulated 10T1/2 cells expressed a smooth muscle cell phenotype, evident from positive staining for α -SM actin (green), and also exhibited 3D extension of pseudopodia (Fig. 3c).

Viability and Proliferative Ability of Encapsulated Cells

Cell viability was quantified for cells encapsulated in three different conditions. In Condition 1, cells were encapsulated as described above, using spatially varied UV exposure (Fig. 1b) to fabricate the four patterns (spiral, pyramid, flower and dome). Condition 2 served as a control slab structure, where all areas received the same UV exposure. In Condition 3, control slab structures were exposed to an additional round of UV exposure using the same mask sets used in Condition 1. Specifically, for Condition 3, the slab structure was polymerized first, rinsed to remove any excess pre-polymer, and then exposed to UV a second time using the four pattern series of masks. Condition 3 was designed to determine if areas with different amounts of cumulative UV exposure alone (in the absence of differences in the 3D geometry of the scaffold) would exhibit cell behavior and proliferative ability in a pattern that corresponds to the UV exposure. This additional experimental condition provides a means to decouple the potentially confounded effects of patterned UV exposure and 3D morphology. As demonstrated by the calcein-AM (green)/ethidium homodimer-1 (red) LIVE/DEAD assay, 10T1/2 cells in all three conditions revealed similar levels of cell viability (Fig. 4a and c).

The Click-iT[®] EdU proliferation assay was used to better characterize the mitotic rates of cells within the scaffolds. At 5 days post-encapsulation, scaffolds laden with 10T1/2s were incubated for 24 h in media containing EdU (5-ethynyl-2'-deoxyuridine), a nucleoside analog of thymidine. Following fixation, Alexa 488 (green) was used to label the EdU via click chemistry to visualize the proliferative cells that had incorporated the EdU during active DNA synthesis. The 10T1/2 cells were counter-stained for α -SM actin (red) and for nuclei (blue) using Hoechst (Fig. 4b). Quantification of proliferation at different quarter-increment heights throughout the scaffold demonstrates height-dependent rates of proliferation (Fig. 4d). We speculate that this height-dependence is caused by diffusion-mediated concentration gradients of metabolites, as cells closer to the scaffold surface

will encounter greater nutrient supply due to their proximity to the concentration boundary layer. This reasoning was further supported by the observation that the patterned scaffolds exhibited greater proliferative activity overall when compared to the slab scaffolds, as the increased surface area provided by the 3D topographic features would also enhance nutrient flux.

Expression of α -SM Actin in Encapsulated 10T1/2 Cells

To determine the long-term influence of 3D cell encapsulation on cell behavior when compared to cell seeding, we prepared cell-encapsulated scaffolds alongside blank scaffolds with seeded cells. However, we observed in our initial experiments that rapid proliferation of cells occurred on the scaffold surface for both the cell-encapsulated scaffolds as well as the cell-seeded scaffolds. To determine the origin of the proliferative surface cells in the cell-encapsulated scaffolds, we performed time-lapse imaging of these scaffolds immediately after fabrication. We observed the presence of motile cells on the scaffold surface as well as on the exposed glass regions of the methacrylated coverslip at the periphery of the scaffold (data not shown). We hypothesized that these motile cells were cells that had adhered residually to the scaffold and glass surfaces without being encapsulated within the GelMA scaffold during polymerization. As the presence of these surface cells would confound results comparing the cell-encapsulated scaffolds with cell-seeded scaffolds, we developed a scaffold wash protocol that uses a brief incubation in trypsin to allow for the removal of these residual cells. Specifically, scaffolds were treated to a brief (\sim 1 min) soak in 0.25% Trypsin/EDTA immediately after fabrication to loosen any cells that were not completely encapsulated. After trypsin treatment, the scaffolds were thoroughly rinsed under a stream of phosphate buffered saline to aid in the removal of any non-encapsulated cells. The efficacy of the trypsin wash in removing residual surface cells is demonstrated in Supplementary Information Figure S2.

GelMA scaffolds were prepared with either seeded or encapsulated 10T1/2 cells to observe differences in α -SM actin expression and organization that may depend on the method of cell incorporation. Seeded cells demonstrated rapid proliferation, and expression of α -SM actin was prevalent throughout the various features of the scaffold. Qualitatively greater expression was observed on the top portions of each of the geometries, and higher levels of expression were localized to distinct features of each of the geometries (Fig. 5a). Encapsulated cells exhibited marked differences in cell morphology as compared with seeded cells (Fig. 5b). Comparatively lower levels of α -SM actin expression were observed for encapsulated cells. After long-term culture, cells demonstrated greater organization around the perimeter of the local structures. Importantly, the cells expressing α -SM actin were located within the interstitial spaces between the structures in the cell-encapsulated scaffolds, whereas smooth muscle-type cells were located on top of the structures for seeded cells. These

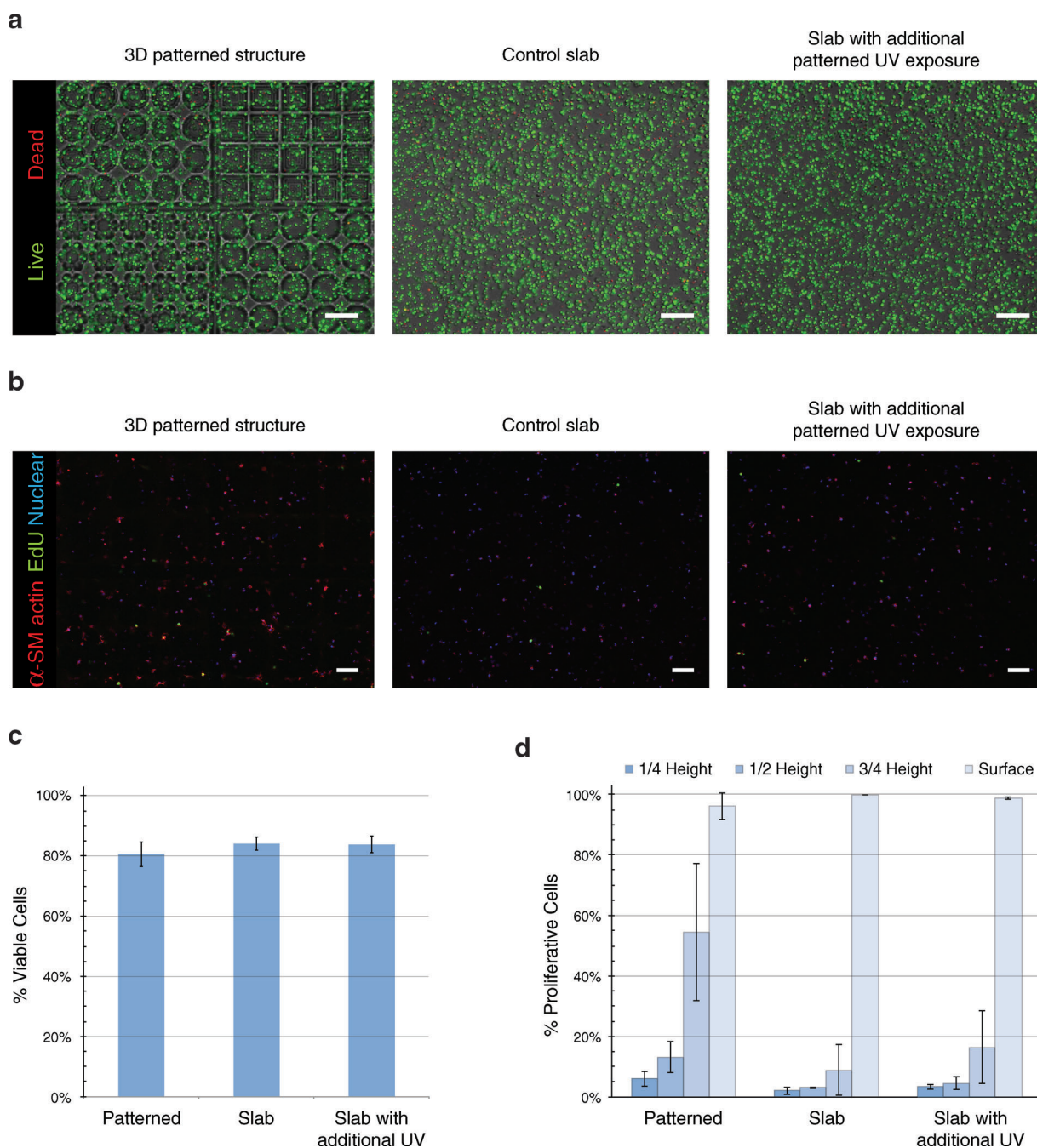


Figure 4. Characterization of cell viability and proliferation. **a:** Viability of 10T1/2 cells encapsulated in GelMA scaffolds was assessed via calcein-AM (green)/ethidium homodimer (red) LIVE/DEAD assay at 8 h after encapsulation. Cell viability within the 3D patterned scaffold was compared to an unpatterned control slab and to a slab that received a second round of UV exposure. These three conditions were compared to determine if differences in cumulative UV exposure alone were contributing to the cellular responses to geometric cues. High cell viability was maintained in all scaffolds, and quantification revealed that similar levels of viability were seen across the three conditions (**c**). The Click-iT[®] EdU assay was performed at Day 5 to assess the proliferative ability of 10T1/2 cells throughout the scaffold (**b**). Incorporated EdU was labeled with Alexa 488 (green) and counterstained for α -SM actin (red) and for all nuclei (blue) using Hoechst. Images shown were taken at a Z cross-section mid-depth within the scaffold. **d:** Quantification of proliferation at different heights throughout the scaffold demonstrates height-dependent rates of proliferation, with cells exhibiting higher proliferation within the 3D patterned scaffold. Labels for the height indicate quarter-increment distances from the base of the scaffold to the scaffold surface (e.g., for a scaffold with total height = 200 μ m, 1/4 height refers to the slice located 50 μ m from the base of the scaffold). Scale bars are (a) 250 μ m and (b) 100 μ m. Error bars represent the SD of three independent samples.

differences in cell morphology and distribution reflect the versatility offered by different methods of incorporating cells as well as the importance of 3D culture in directing cell fate. Furthermore, encapsulation of cells within different 3D

microstructures can allow for the temporally controlled release of cells.

The development of 3D hydrogel cell cultures has undergone a rapid evolution in recent years, and the evidence

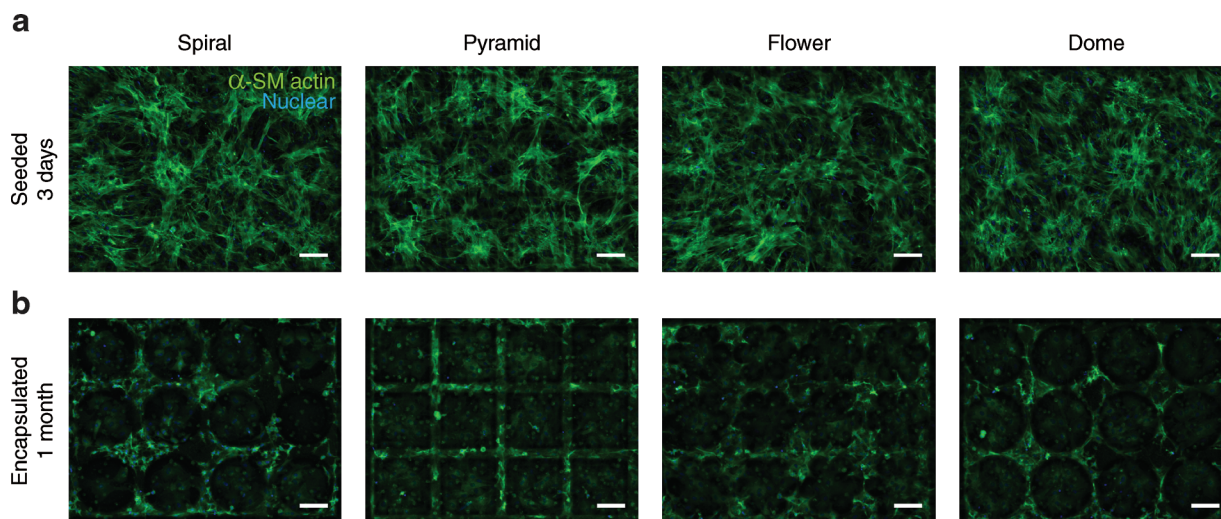


Figure 5. Differences in cell morphology and α -SM actin expression (green) between seeded versus encapsulated 10T1/2 cells in GelMA. Comparison between (a) seeded cells on 3D patterned scaffolds at Day 3 and (b) encapsulated cells after long-term (1 month) culture reveals a more defined geometric response for encapsulated cells along with differences in α -SM actin expression and cell morphology. All scale bars are 100 μ m.

of dramatic differences in cell behavior between 2D and 3D culture systems adds impetus to the transition towards 3D systems for various biomedical applications from drug discovery and cancer research to stem cells and tissue engineering (Chan et al., 2010; Khetani and Bhatia, 2008; Soman et al., 2012; Tung et al., 2011). Efforts to generate a suitable 3D environment for long-term cell culture adopt multiple approaches, including droplet suspension, magnetic levitation, cast molding, lithographic approaches, microfluidics, cell-printing, etc. (Chan et al., 2010; Gaebel et al., 2011; Kaji et al., 2011; Miller et al., 2012; Souza et al., 2010; Torisawa et al., 2009; Tung et al., 2011; Zhang et al., 2012). However, these methodologies are typically limited in their ability to fully replicate the *in vivo* environment either in terms of the material used, the distribution of cells, or the complex geometries of the native physiology. The current state of the art biofabrication technologies face problems related to cell culture such as cell density, cell distribution, integration of multiple cell types and specific localization of cells (Kaji et al., 2011; Kirkpatrick et al., 2011) within a 3D microstructure.

We present a simple and rapid fabrication approach for encapsulating cells within complex 3D geometries using a combination of digital printing and a naturally derived gelatin-based hydrogel. This rapid-fabrication cell encapsulation method demonstrates good cell viability, control over cell distribution, and cell-compatible processing steps with the ability to scale-up towards high-throughput platforms. This technique offers a broad collection of capabilities to explore the independent and interacting effects contributed by different material types, cell arrangements, and feature geometries. These influences may be investigated in the context of cell–cell communication, nutrient diffusion, cell migration, ECM remodeling, and cell differentiation.

Furthermore, the macromer solution used during fabrication can easily be changed to incorporate a variety of bioactive molecules, such as growth factors, drugs, or genetic cues along with multiple cell types. Additionally, each of these macromer variations can be used to provide scaffolds for cell seeding, cell encapsulation, or a combination thereof. As we have demonstrated with the fabrication of a various subset of topographies, virtually any geometry can be constructed. The resolution of the features depends on the material used. For example, using polyethylene glycol diacrylate (MW = 700 Da) without encapsulated cells, an XY resolution of $\sim 6 \mu\text{m} \times 6 \mu\text{m}$ can be achieved, whereas 10% GelMA with encapsulated cells (3×10^6 cells/mL) results in an XY resolution of $\sim 17 \mu\text{m} \times 17 \mu\text{m}$ (Supplementary Information Fig. S3). The resolution in the z direction is much finer (sub-micron range) as this dimension is fabricated while the stage moves continuously through the polymerization focal plane. This work fills a large gap in the field of developing a scalable technique for rapidly fabricating complex 3D cell-laden scaffolds to investigate and regulate cell-topography/geometry/microenvironment interactions towards the goal of directing ultimate cellular phenotype. The platform enables researchers to recreate *in vivo*-like biosystems with complex 3D interfacial arrangements (e.g., blood and lymph vasculature, renal glomeruli, intestinal villi, pulmonary alveoli (Kaji et al., 2011; Kirkpatrick et al., 2011; Yu et al., 2012)), where cells separated in spatially organized zones with specific geometries can exert redundant, competing, or orthogonal influences to collectively regulate the native physiology.

The project described was supported by Award Number R01EB012597 from the National Institute of Biomedical Imaging and Bioengineering and by grants (CMMI-1120795, CMMI-1130894) from the National Science Foundation (NSF) to S.C. Additional funding for P.H.C. was provided by a NSF Graduate Research

Fellowship under grant no. DGE-1144086. We also acknowledge the UCSD Neuroscience Microscopy Shared Facility grant P30 NS047101 for use of confocal imaging.

References

- Bhatia SN, Balis UJ, Yarmush ML, Toner M. 1999. Effect of cell–cell interactions in preservation of cellular phenotype: Cocultivation of hepatocytes and nonparenchymal cells. *FASEB J* 13(14):1883–1900.
- Boland T, Xu T, Damon B, Cui X. 2006. Application of inkjet printing to tissue engineering. *Biotechnol J* 1(9):910–917.
- Chan V, Zorlutuna P, Jeong JH, Kong H, Bashir R. 2010. Three-dimensional photopatterning of hydrogels using stereolithography for long-term cell encapsulation. *Lab Chip* 10(16):2062–2070.
- Chen CS, Mrksich M, Huang S, Whitesides GM, Ingber DE. 1997. Geometric control of cell life and death. *Science* 276(5317):1425–1428.
- Cukierman E, Pankov R, Yamada KM. 2002. Cell interactions with three-dimensional matrices. *Curr Opin Cell Biol* 14(5):633–640.
- Dalby M, Gadegaard N, Tare R, Andar A, Riehle M, Herzyk P, Wilkinson C, Oreffo R. 2007. The control of human mesenchymal cell differentiation using nanoscale symmetry and disorder. *Nat Mater* 6(12):997–1003.
- Du Y, Lo E, Ali S, Khademhosseini A. 2008. Directed assembly of cell-laden microgels for fabrication of 3D tissue constructs. *Proc Natl Acad Sci USA* 105(28):9522–9527.
- Eloumi Hannachi I, Itoga K, Kumashiro Y, Kobayashi J, Yamato M, Okano T. 2009. Fabrication of transferable micropatterned-co-cultured cell sheets with microcontact printing. *Biomaterials* 30(29):5427–5432.
- Fan CY, Tung Y-C, Takayama S, Meyhöfer E, Kurabayashi K. 2008. Electrically programmable surfaces for configurable patterning of cells. *Adv Mater* 20(8):1418–1423.
- Fischbach C, Kong HJ, Hsiong SX, Evangelista MB, Yuen W, Mooney DJ. 2009. Cancer cell angiogenic capability is regulated by 3D culture and integrin engagement. *Proc Natl Acad Sci USA* 106(2):399–404.
- Fraleigh SI, Feng Y, Krishnamurthy R, Kim D-H, Celedon A, Longmore GD, Wirtz D. 2010. A distinctive role for focal adhesion proteins in three-dimensional cell motility. *Nat Cell Biol* 12:598–604.
- Fu J, Wang Y-K, Yang MT, Ravi A, Desai Yu X, Liu Z, Chen CS. 2010. Mechanical regulation of cell function with geometrically modulated elastomeric substrates. *Nat Methods Brief Commun* 7:733–736.
- Gaebel R, Ma N, Liu J, Guan J, Koch L, Klopsch C, Gruene M, Toelk A, Wang W, Mark P, Wang F, Chichkov B, Li W, Steinhoff G. 2011. Patterning human stem cells and endothelial cells with laser printing for cardiac regeneration. *Biomaterials* 32(35):9218–9230.
- Gauvin R, Chen Y-C, Lee JW, Soman P, Zorlutuna P, Nichol JW, Bae H, Chen S, Khademhosseini A. 2012. Microfabrication of complex porous tissue engineering scaffolds using 3D projection stereolithography. *Biomaterials* 33(15):3824–3834.
- Hui EE, Bhatia SN. 2007. Micromechanical control of cell–cell interactions. *Proc Natl Acad Sci USA* 104(14):5722–5726.
- Jeon H, Hidai H, Hwang DJ, Healy KE, Grigoriopoulos CP. 2010. The effect of microscale anisotropic cross patterns on fibroblast migration. *Biomaterials* 31(15):4286–4295.
- Kaji H, Camci-Unal G, Langer R, Khademhosseini A. 2011. Engineering systems for the generation of patterned co-cultures for controlling cell–cell interactions. *Biochim Biophys Acta* 1810(3):239–250.
- Kane RS, Takayama S, Ostuni E, Ingber DE, Whitesides GM. 1999. Patterning proteins and cells using soft lithography. *Biomaterials* 20(23):2363–2376.
- Khetani SR, Bhatia SN. 2008. Microscale culture of human liver cells for drug development. *Nat Biotech* 26(1):120–126.
- Kikuchi K, Sumaru K, Edahiro J-I, Ooshima Y, Sugiura S, Takagi T, Kanamori T. 2009. Stepwise assembly of micropatterned co-cultures using photoresponsive culture surfaces and its application to hepatic tissue arrays. *Biotechnol Bioeng* 103(3):552–561.
- Kirkpatrick CJ, Fuchs S, Unger RE. 2011. Co-culture systems for vascularization—Learning from nature. *Adv Drug Deliv Rev* 63(4):291–299.
- Kulangara K, Leong KW. 2009. Substrate topography shapes cell function. *Soft Matter* 5(21):4072–4076.
- Loessner D, Stok KS, Lutolf MP, Huttmacher DW, Clements JA, Rizzi SC. 2010. Bioengineered 3D platform to explore cell–ECM interactions and drug resistance of epithelial ovarian cancer cells. *Biomaterials* 31(32):8494–8506.
- Malone E, Lipsch H. 2007. Fab@Home: The personal desktop fabricator kit. *Rapid Prototyping J* 13:245–255.
- Miller JS, Stevens KR, Yang MT, Baker BM, Nguyen D-HT, Cohen DM, Toro E, Chen AA, Galie PA, Yu X, Chaturvedi R, Bhatia SN, Chen CS. 2012. Rapid casting of patterned vascular networks for perfusable engineered three-dimensional tissues. *Nat Mater* 11(9):768–774.
- Mironov V, Prestwich G, Forgacs G. 2007. Bioprinting living structures. *J Mater Chem* 17(20):2054–2060.
- Nichol JW, Koshy ST, Bae H, Hwang CM, Yamanlar S, Khademhosseini A. 2010. Cell-laden microengineered gelatin methacrylate hydrogels. *Biomaterials* 31(21):5536–5544.
- Nicodemus GD, Bryant SJ. 2008. Cell encapsulation in biodegradable hydrogels for tissue engineering applications. *Tissue Eng Part B Rev* 14(2):149–165.
- Ovsianikov A, Gruene M, Pflaum M, Koch L, Maiorana F, Wilhelmi M, Haverich A, Chichkov B. 2010. Laser printing of cells into 3D scaffolds. *Biofabrication* 2(1):014104.
- Pampaloni F, Reynaud EG, Stelzer EHK. 2007. The third dimension bridges the gap between cell culture and live tissue. *Nat Rev Mol Cell Biol* 8:839–845.
- Soman P, Kelber JA, Lee JW, Wright TN, Vecchio KS, Klemke RL, Chen S. 2012. Cancer cell migration within 3D layer-by-layer microfabricated photocrosslinked PEG scaffolds with tunable stiffness. *Biomaterials* 33:7064–7070.
- Souza GR, Molina JR, Raphael RM, Ozawa MG, Stark DJ, Levin CS, Bronk LF, Ananta JS, Mandelin J, Georgescu M-M, Bankson JA, Gelovani JG, Killian TC, Arap W, Pasqualini R. 2010. Three-dimensional tissue culture based on magnetic cell levitation. *Nat Nano* 5(4):291–296.
- Tibbitt MW, Anseth KS. 2009. Hydrogels as extracellular matrix mimics for 3D cell culture. *Biotechnol Bioeng* 103(4):655–663.
- Torisawa Y-S, Mosadegh B, Luker GD, Morell M, O’Shea KS, Takayama S. 2009. Microfluidic hydrodynamic cellular patterning for systematic formation of co-culture spheroids. *Integr Biol* 1(11–12):649–654.
- Tung Y-C, Hsiao AY, Allen SG, Torisawa Y-S, Ho M, Takayama S. 2011. High-throughput 3D spheroid culture and drug testing using a 384 hanging drop array. *Analyst* 136(3):473–478.
- Williams CG, Malik AN, Kim TK, Manson PN, Elisseff JH. 2005. Variable cytocompatibility of six cell lines with photoinitiators used for polymerizing hydrogels and cell encapsulation. *Biomaterials* 26(11):1211–1218.
- Wirtz D, Konstantopoulos K, Searson PC. 2011. The physics of cancer: The role of physical interactions and mechanical forces in metastasis. *Nat Rev Cancer* 11(7): 512–522.
- Yeh J, Ling Y, Karp JM, Gantz J, Chandawarkar A, Eng G, Blumling Iii J, Langer R, Khademhosseini A. 2006. Micromolding of shape-controlled, harvestable cell-laden hydrogels. *Biomaterials* 27(31):5391–5398.
- Yu J, Peng S, Luo D, March JC. 2012. In vitro 3D human small intestinal villous model for drug permeability determination. *Biotechnol Bioeng* 109(9):2173–2178.
- Zaman MH, Trapani LM, Sieminski AL, MacKellar D, Gong H, Kamm RD, Wells A, Lauffenburger DA, Matsudaira P. 2006. Migration of tumor cells in 3D matrices is governed by matrix stiffness along with cell–matrix adhesion and proteolysis. *Proc Natl Acad Sci USA* 103(29):10889–10894.
- Zhang AP, Qu X, Soman P, Hribar KC, Lee JW, Chen S, He S. 2012. Rapid fabrication of complex 3D extracellular microenvironments by dynamic optical projection stereolithography. *Adv Mater* 24(31):4266–4270.

Supporting Information

Additional supporting information may be found in the online version of this article at the publisher’s web-site.